

Chapter 2 – Effects of Processing and Temperature on Charpy Impact Toughness in Metallic Glasses and Metallic Glass Matrix Composites

Introduction to Charpy Testing

Charpy impact testing (CIT) is an ASTM standard fracture mechanics technique used to measure a material's notch toughness at moderately high strain rates. It is defined by the ASTM standard E23¹, requiring a 55x10x10 mm beam with a 45°, 2 mm deep notch cut into the midpoint of the 55 mm side (Figure 2-1). The testing apparatus consists of a weighted hammer mounted at the end of a pendulum. The hammer can be raised to a known height and the sample to be tested placed in the path of the hammer's swing, with the notch facing away from the impact surface (Figure 2-2). By measuring the height of the hammer's swing after impacting the sample, a measurement of the energy absorbed by a sample can be taken.

$$\Delta E = mg(h_f - h_i) \quad (1)$$

The lost potential energy is converted into work, which fractures the sample by driving a crack initiating at the notch. The sample geometry, with the notch facing away from the hammer's impact, is used to cause a stress concentration at the tip of the notch to ensure the sample fails instead of bending along the rest of the bar.

While the results obtained from a CIT are not necessarily quantitative by nature, it is a useful tool to make qualitative comparisons between different materials or conditions on a material's toughness. It will not provide a measurement of a quantitative property, such as plane-strain fracture toughness, K_{Ic} .

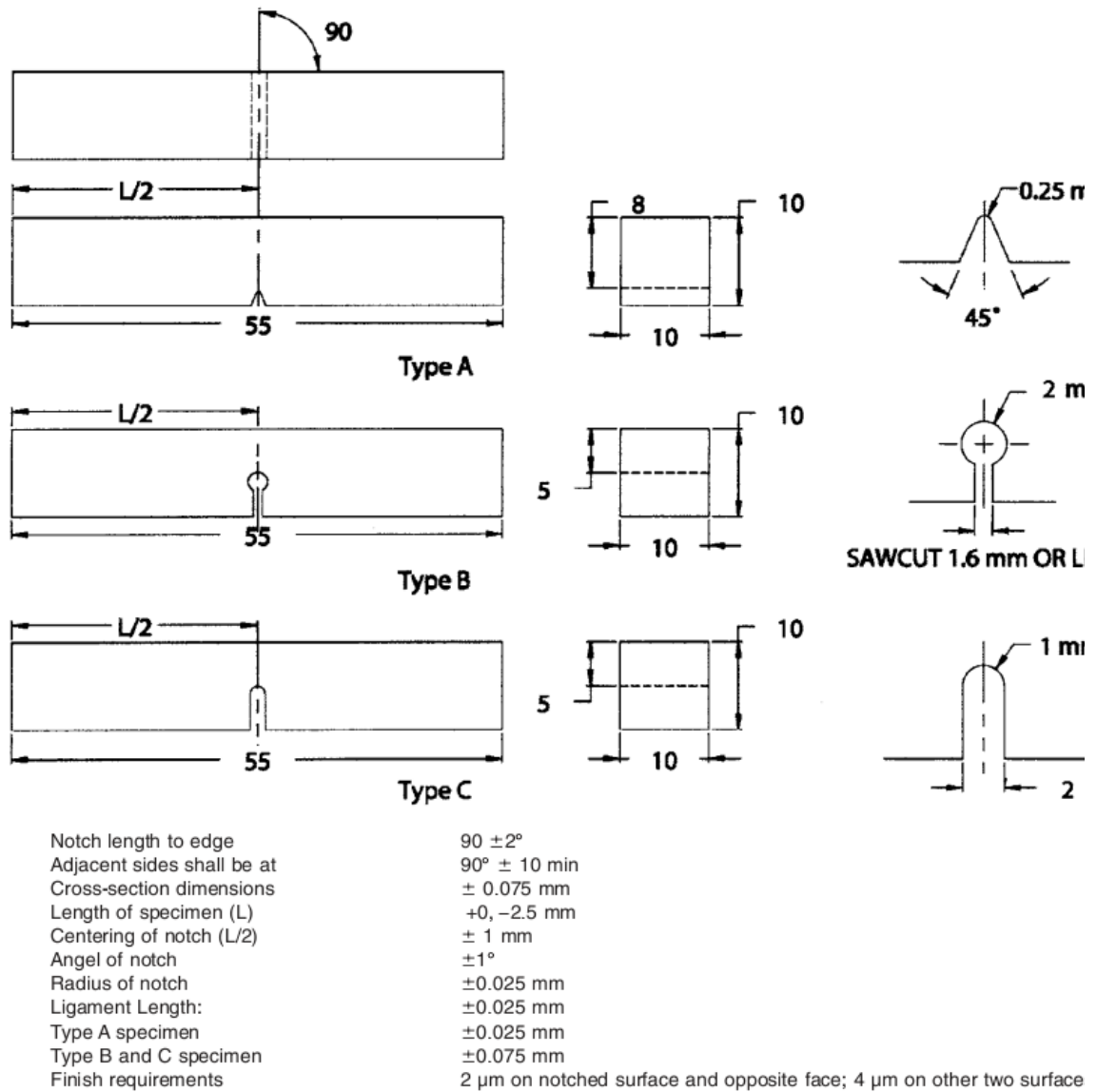


Figure 2-1: Geometry required for an ASTM standard Charpy impact test.¹ Type A is the geometry modified for our testing due to limitation in casting thickness in BMG alloys.

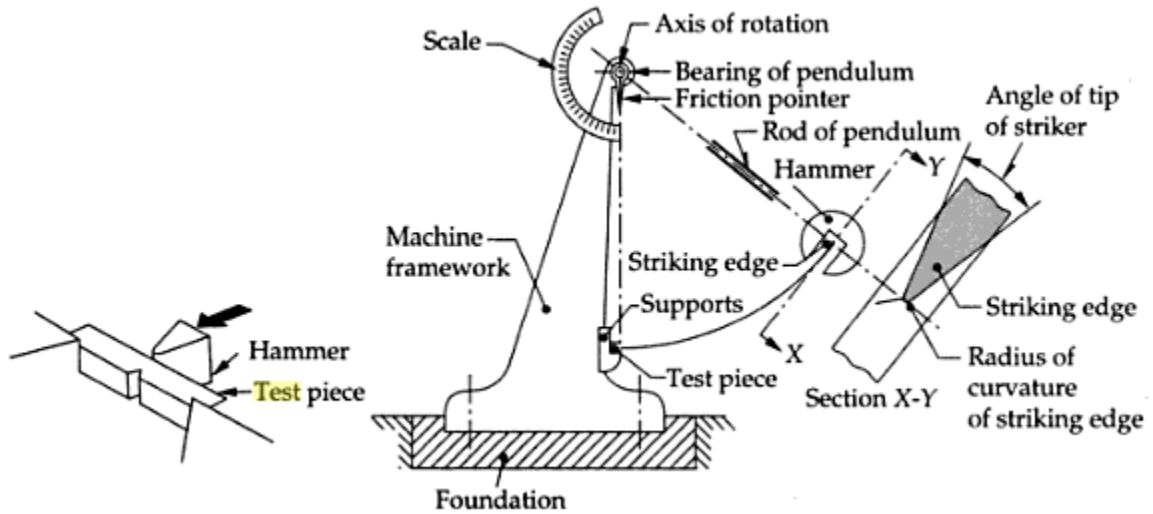


Figure 2-2: A schematic of a Charpy impact test.²

Some materials, upon cooling below a critical temperature, will exhibit a rapid decrease in their measured impact toughness. This change is called a ductile to brittle transition (DTBT). The CIT provides a rapid and reliable method to measure the relative change in impact toughness of a material as it becomes more brittle. This is primarily because the CIT test can be performed in a matter of seconds after removing a test specimen from a cryogenic bath or oven, allowing the entire test to be performed isothermally. In contrast, a plane-strain fracture toughness test would have to be performed in an environmental chamber for non-ambient temperature testing. It is known that fcc materials do not undergo a DTBT, while bcc and hcp metals do. Some cryogenic work has been done on BMGs to assess their ambient impact toughness, as well as their elevated and cryogenic toughness. Two Charpy studies were performed by Raghavan et al.^{3,4} where in one study the BMG Vitreloy 1 was tested from 100 K to 450 K, and in the other the samples were annealed and then tested from 100 K to 600 K. Toughness was shown to dramatically decrease with increasing temperature in both studies. H Li et al.⁵ performed compression tests of a Zr-based BMG at 77 K and observed an increase in

the compressive yield strength compared to room temperature, while Huang et al.⁶ saw both an increase in compressive strength and plasticity at 123 K. Yu et al.⁷ studied the temperature dependence of the various elastic moduli at cryogenic temperatures. Qiao et al.⁸ summarized the ultimate tensile strength of BMGs from 75 to 300 K. Not surprisingly, the properties of BMGs remain relatively unchanged even at cryogenic temperatures. The toughness does decrease with temperature, but in a linear fashion similar to fcc metals, instead of the sharp order-of-magnitude drop associated with bcc metals and those with a DTBT.

Although the toughness of BMGs doesn't decrease significantly at cryogenic temperatures, their initial toughness is fairly low compared with most high-performance engineering materials (e.g. titanium, steel, and aluminum alloys). To address this shortcoming, bulk metallic glass matrix composites (BMGMCs) have been developed to offer significantly higher toughness at room temperature due to the ability of a soft, bcc crystalline phase to stop shear band propagation. Qiao et al.⁸ performed compression tests on two BMGMCs to observe if the embedded bcc crystalline dendrites exhibited an expected DTBT temperature. In both alloys there was significant compressive plasticity at room temperature, but at 77 K the sample was brittle. Unfortunately, only two temperatures were measured (room temperature and 77 K), so there was not enough information to confirm or reject the existence of a DTBT in BMGMCs. In this chapter, measurements were performed at ten different temperatures ranging from 100 K to 300 K to allow for a more complete view of how impact toughness varies with temperature. Using impact testing instead of compressive testing is also preferred, as plasticity can be influenced by frictional forces during compression tests. Compression tests are also slow, making it difficult to maintain isothermal conditions throughout the test.

Charpy tests were also performed on a variety of BMGs and BMGMCs that were prepared using different processing conditions. This was done to provide a baseline for further Charpy testing of both BMGs and BMGMCs that cannot be formed into the shapes required for larger mechanical tests. This chapter also represents the first Charpy study of BMGMCs, done to compliment work done in the literature with quasistatic and dynamic mechanical testing.⁹⁻¹⁴

Experimental

This chapter focuses on comparing the impact behavior of three BMGMCs to Vitreloy 1 (a monolithic BMG) as well as some traditional crystalline alloys. The first BMGMC tested is a titanium-based alloy DV1 ($\text{Ti}_{48}\text{Zr}_{20}\text{V}_{12}\text{Cu}_5\text{Be}_{15}$), with 40% crystal volume fraction. The second is a zirconium-titanium-based alloy DH3 ($\text{Zr}_{39.9}\text{Ti}_{33.9}\text{Nb}_{7.6}\text{Cu}_{6.4}\text{Be}_{12.5}$), with 67% crystal volume fraction. LM2 ($\text{Zr}_{71.9}\text{Ti}_{9.3}\text{Nb}_6\text{Cu}_{6.15}\text{Ni}_{4.6}\text{Be}_{1.6}$), a commercially available zirconium-based composite material, is 40% crystalline. Vitreloy 1 ($\text{Zr}_{41.2}\text{Ti}_{13.8}\text{Cu}_{12.5}\text{Ni}_{10}\text{Be}_{22.5}$) is the BMG used for comparison, and is the most widely commercially used BMG (under the trade name LM1). Several crystalline alloys were also used for comparison with the BMG alloys. These include Ti-6Al-4V, Al-7075, Al-2024, and SS 304. To measure ductile to brittle transitions, both 99.9% pure tin and DH3-Matrix ($\text{Zr}_{35}\text{Ti}_{30}\text{Cu}_{8.25}\text{Be}_{26.75}$), a BMG with composition equivalent to that of the glass matrix in DH3, are used. A summary of their properties can be seen in Table 2-1.

BMG alloys were produced by arc melting high purity elements in a Ti-gettered argon atmosphere. Suction cast (SC) samples were then remelted in a mini-arc melter and cast into 3x3x30 mm beams. A notch 0.5 mm deep, 1 mm wide, 90° cut was made using an endmill. Semi-Solid Forged (SSF) samples were held isothermally above their solidus temperatures prior to forging to allow for dendrite coarsening before being formed into 3 mm thick plates. The plates were then sectioned on a laboratory saw and notched with an endmill similar to the SC samples.

Commercial alloys were procured as 3 mm thick plates, sectioned, and notched in a similar manner.

Charpy tests were performed on a modified Riehle Impact Testing Machine, which was instrumented to detect small changes in hammer velocity (Figure 2-3). Standard Charpy machines operate from two drop heights, 61 and 122 cm (24 and 48 in), with two hammer masses so that four maximum impact energies can be obtained: 41, 81, 163, and 325 J. Unfortunately, full-sized Charpy testing on Zr-Be-based BMGs from literature indicate only 1-5 J of energy is absorbed, whereas Zr-Be-based BMGMCs absorb 25-45J.^{3,4,15-17} Full sized Charpy specimens can be very difficult to fabricate out of various BMGs. A very large critical casting thickness is required, and ingots of at least 30 g would be required (very difficult with laboratory-scale equipment). Changing the sample geometry to 30x3x3 mm allows for rapid fabrication through suction casting in a mini arc melter. In the future, poor glass formers can also be directly compared, since this is an easier geometry for fabrication. Since the impact toughness of the BMG alloys is relatively low, plane-stress effects are absent even in the smaller beams, which means comparisons to tests done in larger specimens are proportional. The cross-sectional area of the compact samples in the current work is approximately 10 times smaller than full-sized samples, so the amount of energy absorbed would be nearly undetectable using standard drop heights and hammer masses. Therefore, the Charpy tester was modified by reducing the drop height and the hammer mass, and the impact energy was measured both by dial and by instrumentation. Equating the potential energy of the hammer at the drop height ($PE=mgh$) with the kinetic energy of the hammer at impact ($KE = mv^2/2$), the initial velocity (v_0) of the hammer before the impact is found to be a function only of the initial drop height.

$$v_0 = \sqrt{2gh} \quad (2)$$

To instrument the machine, a 1 cm diameter cylindrical magnet was attached to a plastic arm on the side of the hammer pendulum. Two 1 cm diameter copper coils were mounted on a plate 70 mm apart, with their midpoint located at the impact location Figure 2-3a. The coils were wired to a digital oscilloscope connected to a computer. When the magnet attached to the hammer passes the first coil, a voltage that registers as a sinusoidal peak on the oscilloscope is created. During the impact with the specimen, the hammer slows down before it passes the second coil, creating a difference in the width of the sinusoidal peak. The energy absorbed by the sample can then be determined through

$$E = \frac{1}{2} m (v_0^2 - v_f^2) \quad (3)$$

The velocity of the hammer can be determined by $v = \Delta x / \Delta t$, where Δt is the width of the sinusoidal pulse (the transit time of the magnet across the coil) and Δx is the width of the coil. Using the known standard drop height of the hammer, the initial velocity was calculated to be 3.46 m/s; using this known velocity, Δx was calculated to be ~1.0 cm for each coil by measuring the peak width. Using the known original impact energy and hammer height, the original effective mass of the hammer was calculated as 6.8 kg. An example of this procedure is demonstrated in Figure 2-3d. To accommodate the small-scale specimens, the energy of the hammer was reduced by decreasing the hammer mass to 2.7 kg and the initial velocity to 2.0 m/s. The new drop height was calculated to be 21 cm (from the measured velocity) and, thus, the total energy of the hammer was reduced from 41 to 5.6 J. For samples requiring more than 5 J to fracture, a second drop height was calibrated at 83 cm, imparting 22.2 J of energy at impact. A modified fixture to support the shorter samples was built as an insert into the existing

Charpy fixture, as shown in Figure 2-3b. The span length was thereby reduced from 50 to 20 mm for the small-scale tests.

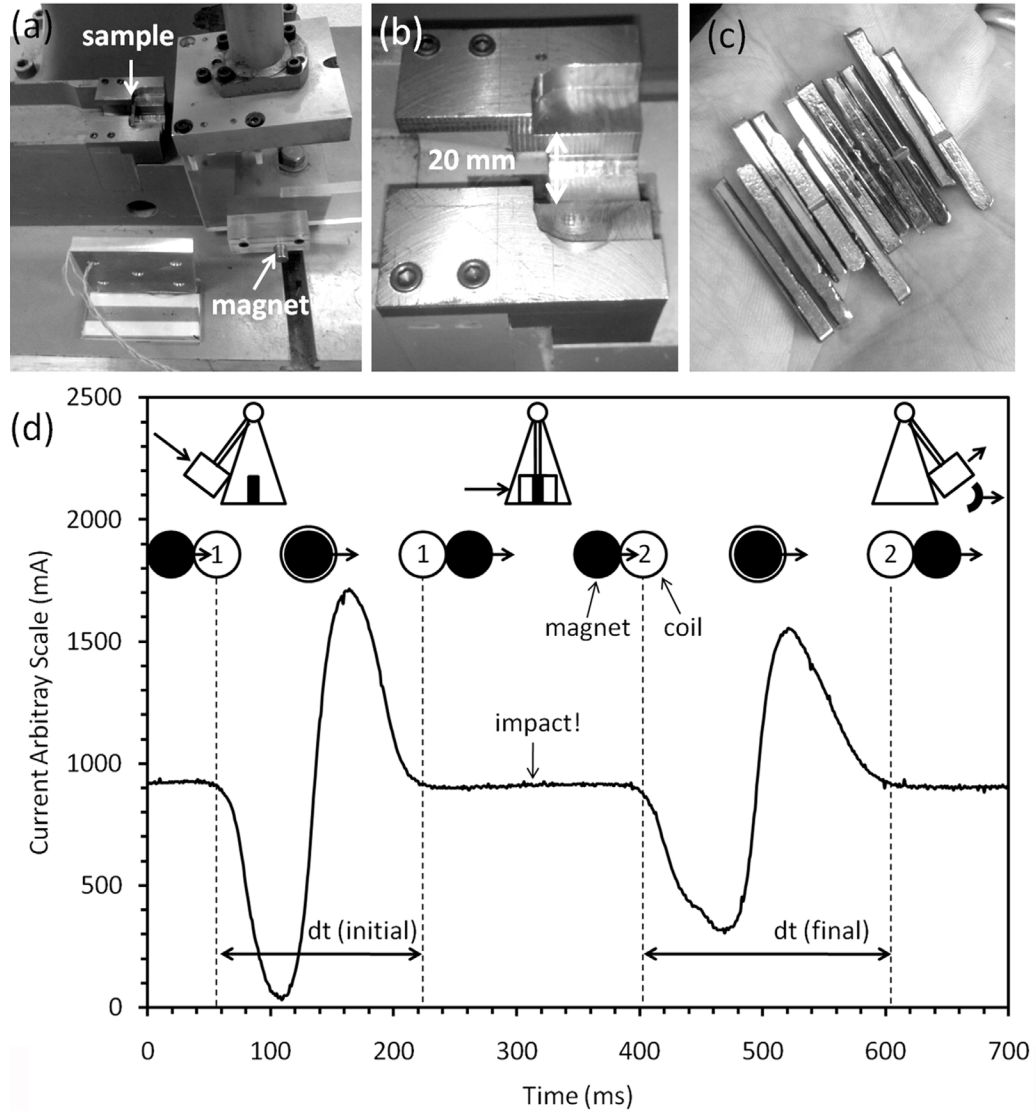


Figure 2-3: Instrumented small-scale Charpy testing. (a) The pendulum hammer has been stripped of excess mass to reduce the impact energy. A plastic extension has been built to hold the magnet. As the pendulum swings, the magnet passes a coil before and after impact, which registers a current. (b) The modified sample holder has a shorter span length of 20 mm for compact Charpy samples. (c) Suction cast (SC) samples of the alloy DV1. (d) Induced current obtained from an impact test on DH3 using a digital oscilloscope. The hammer's speed is reduced during impact, which broadens the second peak. The width of the coils and magnets are known to be $dx = 1$ cm, so the velocity of the hammer can be determined through $v = dx/dt$. The energy during the impact is $E = 1/2 mv^2$.

To calibrate the impact temperatures for the DTBT measurements, a series of heating curves was measured for each alloy. This was done by attaching a thermocouple to a specimen, holding the sample in liquid nitrogen until it reached equilibrium, quickly loading the sample into the testing setup, and then recording the temperature as a function of time as the sample heated due to contact with air and the sample fixture. This was repeated several times for each sample, so a plot of temperature vs. time could be obtained for each sample. The heating curve for DH3 is shown in Figure 2-4. The validity of the testing setup for measuring DTBT was verified by measuring an accurate DTBT temperature for 99.9% Sn.

Microstructures of the samples were analyzed through x-ray diffraction, backscattered scanning electron microscopy (QBSD-SEM), Rockwell hardness testing, acoustical measurements, and optical microscopy.

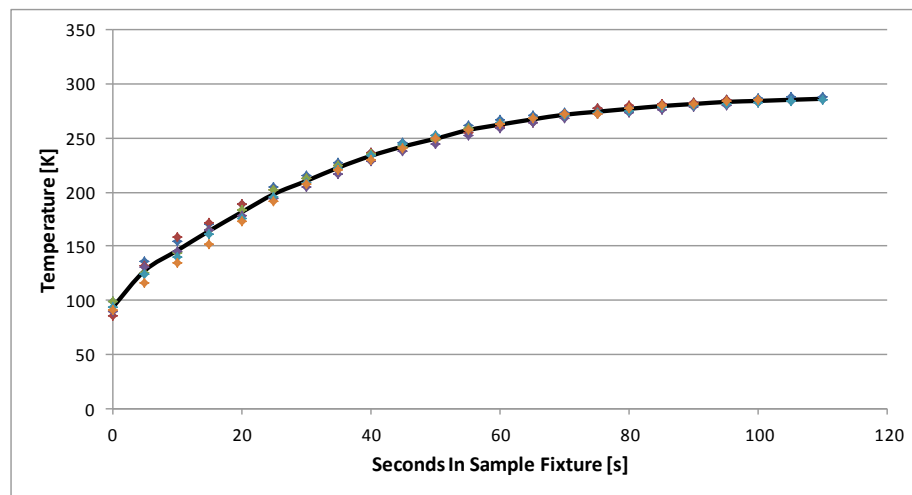


Figure 2-4: The temperature calibration curve for DH3 ($Zr_{39.9}Ti_{33.9}Nb_{7.6}Cu_{6.4}Be_{12.5}$).

Table 2-1: Physical & mechanical properties of samples measured via Charpy impact testing.

Name	Vol % of Crystal	Processing Method	CIT 300 K [J]	CIT 100 K [J]	CIT 300 K [J/cm ²]	CIT 100 K [J/cm ²]	σ_y [MPa]	σ_{max} [MPa]	Hardness [HRc]	ρ [g/cm ³]	E [GPa]	σ_{max}/ρ
Vitreloy 1	0	SC	0.68	0.31	7.6	3.4	1700	1700	60	6.1	97.2	279
LM2	40	CCP	0.13	-	1.4	-	1000	1300	56.2	6.2	78.8	210
DV1	40	SC	1.31	0.33	14.6	3.7	1360	1430	58.3	5.2	92.4	275
DV1	40	SSF	4.82	-	53.6	-	1360	1430	50.8	5.2	92.4	275
DH3	67	SC	2.66	0.32	29.6	3.6	1100	1200	47.8	5.8	75.3	207
DH3	67	SSF	5.27	-	58.6	-	1100	1200	43.3	5.8	75.3	207
DH3-Xtal	100	X-tal	0.19	0.26	2.1	2.9	-	-	-	5.8	-	-
Ti-6-4	100	GD 5 STA	2.97	-	33	-	1100	1200	41	4.5	114	267
Al7075	100	T6	0.38	-	4.2	-	500	570	6	2.8	71.7	203
Al2024	100	T6	0.66	-	7.3	-	350	430	<1	2.8	72.4	155
SS 304	100	STA	9.49	-	105.4	-	220	500	<1	8	190	63
Sn 99.9%	100	X-tal	0.92	0.04	10.2	0.4	12.5	220	<1	5.8	41.4	38

σ_y , σ_{max} , and E for all crystalline alloys (other than DH3-matrix) were obtained from matweb.com. Processing routes for metallic glasses are defined as: SC (suction cast), CCP (commercially cast plate), and SSF (semisolid forged). CIT is Charpy impact toughness.

Results and Discussion

Influence of Processing Conditions of Charpy Impact Energy

Compact Charpy impact testing was performed on a total of 12 alloys: six containing an amorphous phase and six fully crystalline alloys. Table 2-1 gives compositions and processing conditions for the alloys tested. Figure 2-5 is a visual plot of the data in Table 2-1, which shows the impact energy (in Joules) for each sample along with impact energy per cross-sectional area (in J/cm²). On average, seven samples of each type were impacted to observe the effect of processing variation on impact energy, and the mean value for each alloy is shown in Figure 2-5 with a red circle. As a baseline, the monolithic BMG Vitreloy 1 (abbreviated Vit 1) was also evaluated via Charpy testing, as was done by several other groups.^{3,4,16,17} Vit 1, which is the most widely studied and commercialized BMG to date (often under the trade name LM1), is approximately the amorphous matrix for the commercial composite LM2. Commercial quality alloy was obtained and were then broken up and suction cast into beams. The impact energy for the Vit 1 samples was determined to be 0.68 J, which is similar to the results from other studies when scaled to full size, despite differences in sample geometry and origin. The crack propagation through Vit 1 test samples also appears similar to the crack propagation through a fracture toughness tests done in other studies.¹⁵

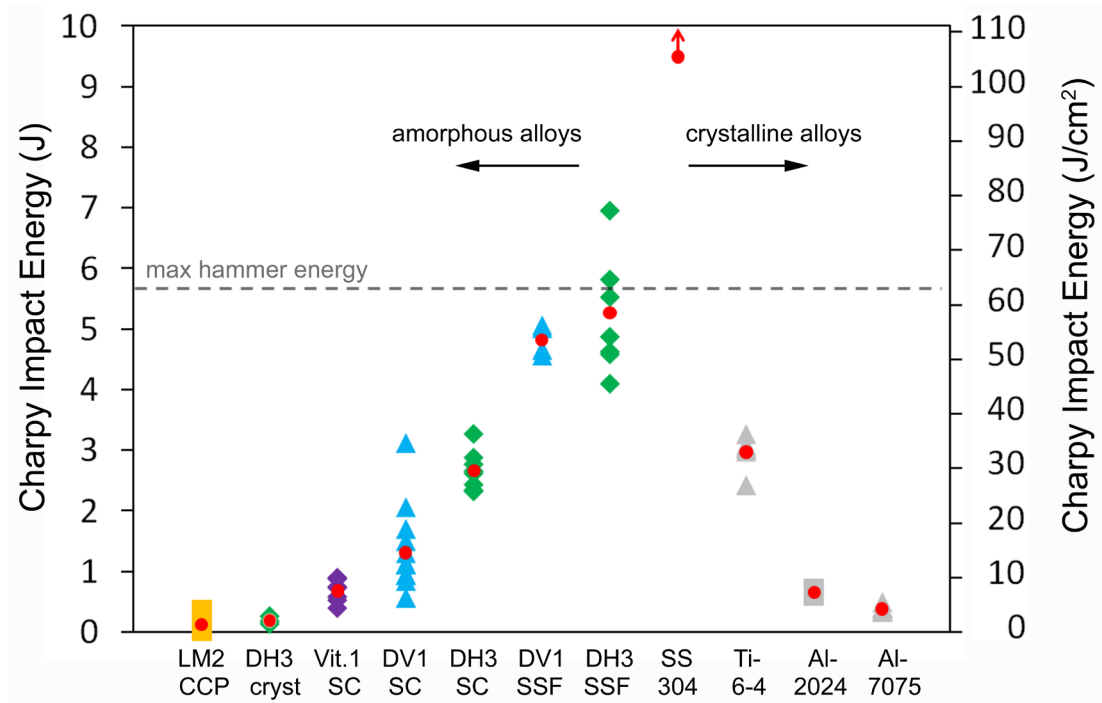


Figure 2-5: Compact Charpy impact toughness values from 11 alloys tested; one bulk metallic glass (BMG), six bulk metallic glass matrix composites (DH3, DV1, LM2) in various processing conditions, and four crystalline alloys. The processing conditions are commercially cast plate (CCP), crystalline (xtal), suction cast (SC), and semisolidly forged (SSF). The maximum hammer energy for the low drop height is displayed on the plot along with a scaled estimation of the full-sized Charpy toughness. On average, seven samples of each alloy were tested, and the average is plotted as a red circle.

Surprisingly, the commercially cast composite, LM2, had the lowest impact energy, with only 0.13 J absorbed. This is in spite of the alloy having approximately 40% volume fraction of a soft, crystalline dendrite phase. The brittle fracture surface typical of an the impact test is shown in Figure 2-6 and the microstructure is shown in Figure 2-7. Images of the fracture surface allow for an estimation of toughness. Qualitative estimates on the toughness of an alloy can be made by inspecting the fracture surface. High surface roughness, large numbers of shear bands, and the shear bands forming a long distance from the fracture surface are all indicative of a tough material. LM2's lack of roughness on the facture surface is indicative of a brittle material, which the impact energy measurements verify. It is well-known from other studies that commercially available LM2 contains a high ppm concentration of oxygen, which reduces the toughness of the matrix BMG considerably. This is the likely cause of the low observed toughness, despite the presence of the dendrites. Cracks forming in the matrix propagated without plastic shielding from the dendrites.

Figure 2-7a is a composite SEM micrograph of LM2 obtained via a quadrant backscatter detector (QBSD). This causes the dendrites to appear white in color versus the gray of the matrix due to the different composition, stemming from the Z-scattering differences. These samples were commercially produced by die-casting a liquid from a shot sleeve into a steel mold. This method has a relatively slow cooling rate, which allowed the microstructure to coarsen to levels similar to the SSF DV1 and DH3samples (shown in Figure 2-8a and Figure 2-9a). The dendrite arms are $\sim 10 \mu\text{m}$ thick, and the spacing of the arms is between 1-5 μm . The main branches of the dendrites are $\sim 100 \mu\text{m}$ in diameter, and are spaced several hundred microns apart. Unlike the other SSF samples, though, LM2 is not extensively toughened by the coarsening, as the crack cleaved through the sample without any significant branching or blunting. A limited number of shear bands can be seen on the surface normal to the fracture, but they only extend between

5 μm to 50 μm away from the crack. As expected, the low commercial purity of the alloys makes the matrix brittle and limits the glass forming ability of the alloy. This causes some brittle intermetallic phases to nucleate during solidification, as seen in Figure 2-7c. In combination, the high-oxygen matrix and the presence of the brittle intermetallic phases result in a very low toughness.

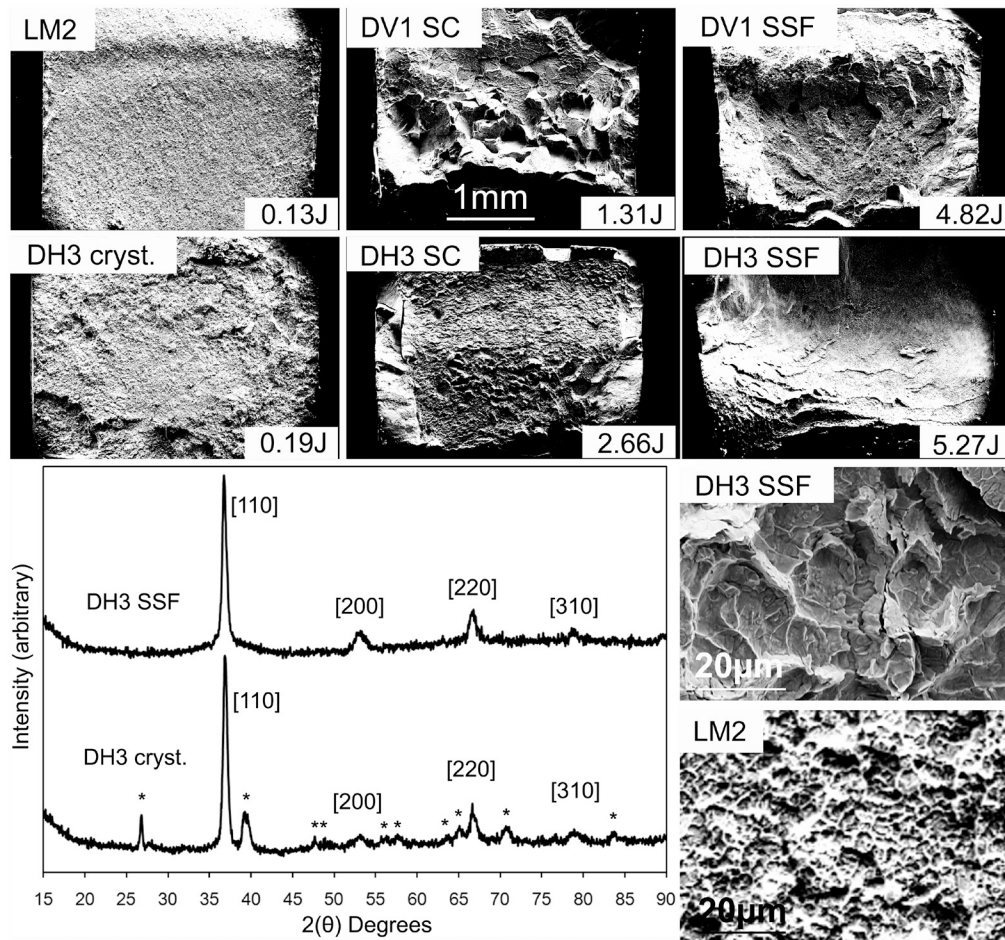


Figure 2-6: Fracture surfaces from six BMGMC samples tested in this study, along with their impact energy. X-ray scans from SSF DH3 and the completely crystalline state are also shown. Although the body-centered cubic dendrites remain in the crystalline sample, the matrix is no longer amorphous, as evident from the numerous starred peaks. Also shown are magnified fracture surfaces from SSF, DH3, and LM2, showing the difference in the fracture pattern. All images are of the fracture surface taken with backscattered electrons in a SEM.



Figure 2-7: (a) A backscattered SEM micrograph showing a fractured specimen of commercially cast LM2. Despite the large, coarse dendrites, other factors (like oxygen content and partial crystallization) make this the most brittle alloy tested. (b) The edge of the crack from a region in (a) demonstrating very little toughness. (c) Another region near the edge of the crack showing that several shear bands have formed. (d) A region where the matrix has crystallized into an unknown brittle phase.

The Ti-based BMGMC DV1 was the first non-commercial composite tested. It is notable for its large amount of tensile strain to failure (~15%) and low density (5.17 g/cm³).¹⁵ Ten samples were suction cast, and their impact energy is plotted as the blue triangles in Figure 2-5. SC DV1 has a large amount of variability, with impact energies between samples spanning nearly an order of magnitude (a low of 0.56 J, high of 3.1 J, and an average of 1.3 J). This is likely caused by the suction casting method, during which molten material is sucked into a mold and there is the possibility of small voids due to the turbulent flow. There are also inconsistencies in the solidification behavior of various DV1 samples as fabrication conditions do not permit identical castings. Temperature control is not perfect, so some would be cast from higher temperatures causing a slower cooling rate and larger dendrites. This would not have been as much of a problem for SC Vit 1, since it lacks the dendritic microstructure seen in the composites and has less variability when cast. To study the effects of dendrite refinement on DV1, an ingot was heated into the semi-solid regime (~950 °C), and held isothermally for ~1 minute to coarsen the microstructure, then forged between two copper plates into a 3mm thick plate (as demonstrated in Ref 18). Semisolidly forging DV1 had a significant effect on impact toughness, with the average energy absorbed increasing by nearly four times to 4.8 J. Scatter was also reduced as a function of both the coarsened microstructure and that the samples were cut from the same plate. Figure 2-8 demonstrates the difference between fractures in the two methods of processing DV1. Both samples exhibit a rough fracture surface, but the SSF sample exhibits significant shear lips on the edges perpendicular to the notch. Figures 2-8a and 2-7d show composite images of the crack path through the DV1 SSF and SC samples, respectively. The microstructure for the SSF sample is actually visible to the unaided eye, as a result of the coarsening imparted by semi-solid processing. Damage can be seen 1-2 mm away from the crack edge, and mostly consists of closely spaced shear bands (<10 μm separation) with significant

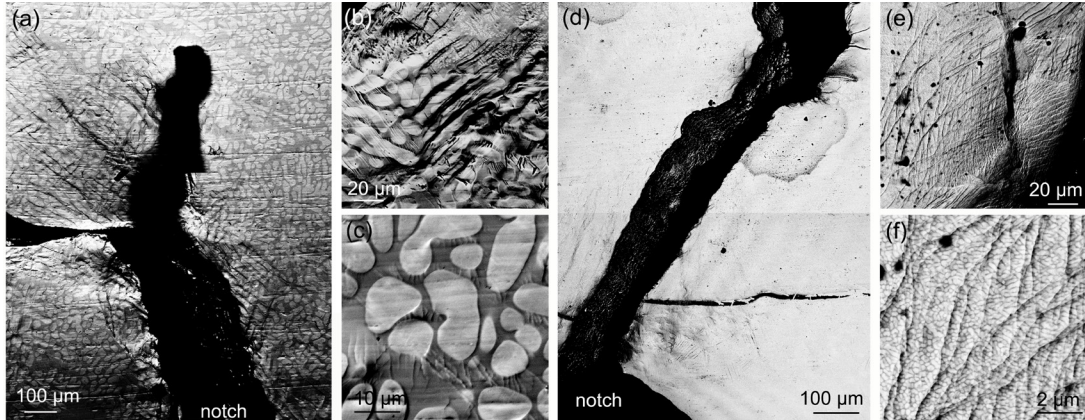


Figure 2-8: Backscattered SEM micrographs from the BMGMC DV1 (40% dendrite). (a) Crack originating at the notch and then propagating through a SSF sample during a compact Charpy test. (b),(c) Higher magnification of shear bands interacting with the Ti-based dendrites (e) Crack propagating through a SC sample during compact Charpy test. (e),(h) Higher magnification micrographs of shear bands in the SC sample along with the nominal microstructure.

damage visible in the dendrites (Figure 2-8b and Figure 2-8c). Dendrite arm spacing is 5-10 μm , with thicknesses \sim 10-15 μm . The length of a dendrite is \sim 100 μm , and the arm spacing is only a few microns. In contrast, the SC sample shows much less branching and blunting, with shear bands only observed \sim 100-200 μm from the edge of the crack. Although many shear bands are observed (Figure 2-8f) compared to an alloy such as Vit 1, there are significantly less than in the SSF sample. The microstructure from the SC sample (Figure 2-8f) is an order of magnitude smaller than the SSF sample, as a result of casting from above the liquidus and rapid quenching. The overall dendrite size is only a few microns, with the arms themselves being approximately 0.5-1 μm . Figure 2-8f is a highly magnified image of the dendrites with shear bands that occurred during fracture. It should be noted that although the SC sample of DV1 had energy absorption 25% less than that in the SSF sample, it is still not a brittle fracture when compared to LM2 and Vit 1. SC samples of DV1 still exhibit ten times higher impact toughness than commercial LM2. Thus, even though the small dendrites aren't as effective at blunting and redirecting the crack tip as the coarser dendrites, they still require a significant amount of energy to fracture.

DH3, the Zr-Ti based BMGMC, was the next impact tested composite. This alloy is notable for its high fracture toughness ($>173 \text{ MPa m}^{1/2}$) and fatigue endurance limit (25% of yield strength), mostly caused by the increased volume fraction of soft dendrites (66%).¹⁵ DH3 specimens were SC and SSF, similar to DV1, but in addition one set of samples intentionally had the matrix crystallized (DH3-xtal) by slowly cooling from the semi-solid region (XRD scan shown in Figure 2-6). The XRD scan from DH3 is a typical scan for all of the composites which exhibit both a large, broad amorphous hump as well as bcc diffraction peaks. The DH3-xtal XRD scan shows how upon the matrix's crystallization, additional diffraction peaks can be seen from the formation of intermetallic phases. XRD scans of other alloys are not shown.

The SC samples of DH3 show the reverse trend during impact testing compared to the SC samples of DV1. Instead of a large scatter, the impact energies are clustered closely to the average of 2.7 J. It is likely due to the higher dendrite fraction (and thereby higher liquidus temperature) that the mini arc melter was unable to fully melt the alloy prior to suction casting, and as a result some dendrite refinement was allowed to take place. This created a more uniform microstructure during casting, which should result in less scatter in impact energies. The SSF DH3 samples also exhibited significantly higher average impact energies than the SC samples (5.4 J), although the improvement was not as dramatic as with DV1. The amount of energy absorbed by SSF DH3 was actually high enough that a larger drop height was required to break the samples. Similarly to DV1, the microstructure difference in DH3 SC and SSF varied by approximately an order of magnitude. The nominal microstructure from the SSF samples is shown in Figure 2-9b and Figure 2-9g, with dendrite arms 10-15 μm wide and spaced $\sim 5 \mu\text{m}$ apart. The overall dendrite size is 100-200 μm . The scale of both DV1 and DH3's SSF samples are similar, with DH3 having a larger fraction of dendrites. In contrast, the dendrites from SC DH3

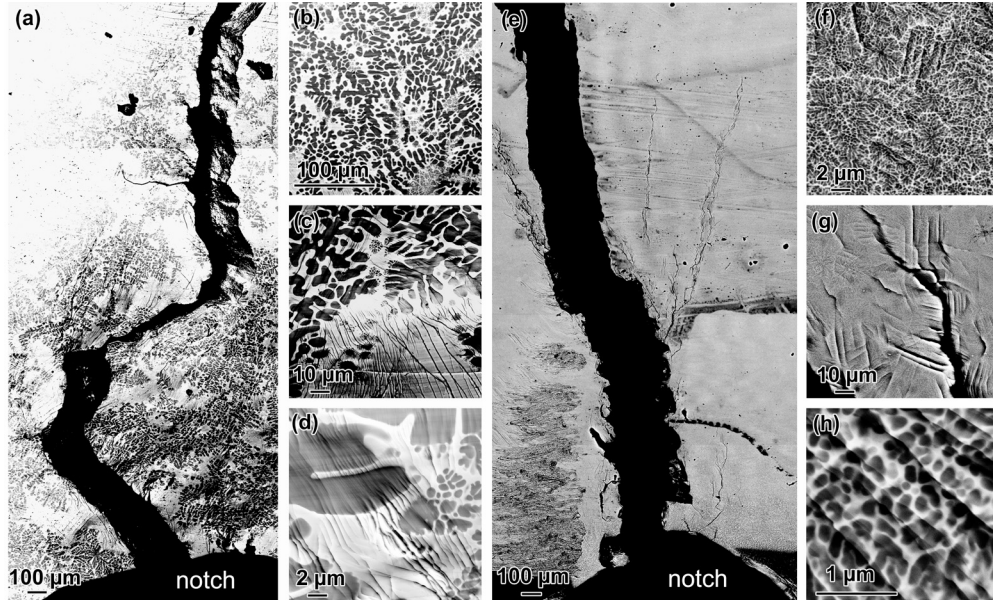


Figure 2-9: (a) Crack arrest and branching after impact in a SSF sample. (b) Near the edge of the crack, many shear bands have formed and been arrested by the soft dendrites. (c) Magnification of a region in (a) demonstrating that even far away from the crack, shear bands still form in the glass matrix. (e) Crack propagating through a SC sample of DH3 and (f),(g) higher magnification images of the shear bands and microstructure.

have an arm size of 0.5-1 μm , and a spacing of only a few hundred nanometers (Figure 2-9f and Figure 2-9h). The overall dendrite size is on the order of 1-5 μm in diameter.

Four common crystalline alloys were also tested in the same geometry for direct comparison with the amorphous alloys, since a smaller than standard Charpy size was used. The aerospace aluminum alloys Al-2024-T6 and Al7075-T6 exhibited impact energies of 0.66 and 0.38 J, with very low observed scatter. Ti-6-4's impact energies were close to that of the SC samples of DH3, but were surpassed by both SSF samples of DV1 and DH3. The fourth crystalline alloy tested was a completely crystallized sample of DH3. It was fabricated via SSF, then annealed in a radio frequency (RF) induction coil until crystallization was visible on the surface. Crystallinity was verified by XRD (Figure 2-6), and no amorphous content was detected via differential scanning calorimetry (DSC). It is not pictured, but the microstructure of the sample is

similar to Figure 2-7d: there are large coarsened dendrites, but the amorphous matrix is replaced by a fine eutectic. Crystallizing the matrix resulted in a measured impact energy of 0.19 J. This is approximately 7% of the SC samples, 3% of the SSF samples, but still higher than the 0.13 J of the LM2 BMGMC. These results underline the importance of ensuring a vitrified and tough matrix. By crystallizing the glass, the impact toughness of the matrix goes down substantially, with a corresponding decrease in the critical size at which cracks form (100 μm in the glass to ~ 10 nm in the crystalline eutectic.¹⁵). Since self-propagating cracks form at such small lengths in the crystalline matrix, the dendrites, regardless of size, have no effect on toughening, since cracks simply bypass them and propagate through the matrix unhindered. DH3's 67% volume fraction of crystal still experiences an order of magnitude decrease in toughness when the matrix is crystallized. Figure 2-6 shows fracture surfaces of all DH3 samples (SC, SSF, xtal) along with higher magnification images comparing the dimpled fracture pattern between tough SSF DH3 and brittle LM2 samples. As expected, the brittle sample exhibits approximately an order of magnitude smaller dimple pattern than the toughest composite alloy (~ 20 μm versus ~ 2 μm). The fracture surfaces from the composites in order of increasing toughness from the crystalline DH3 sample to the SC sample, to the SSF sample. In each case, the roughness increases with toughness, as does the size of shear lips on the sample's edge (nearly 1mm in SSF DH3).

Finally, rolled samples of 304 stainless steel were tested, resulting in an average impact energy of 9.5 J. These samples exhibited sufficiently high toughness in that the hammer was not able to easily fracture the samples. This caused the hammer to vibrate significantly, and likely added to large error in measurement. Because of this, only the average value is plotted in Figure 2-5.

Ductile to Brittle Transition in BMGMCs

To investigate the presence of a DTBT temperature in BMGMCs, further Charpy impact testing was performed from room temperature down to liquid nitrogen temperatures. Figure 2-10 plots the measured impacted energy versus the temperature of the sample at time of impact. As in the previous tests, where crystalline alloys were impact tested to verify the setup, in this section pure Sn was impacted to verify that the DTBT temperature is similar to what is measured in full-sized specimens. The Sn 99.9% curve recreates that from the literature¹⁹ well, with a roughly linearly decreasing toughness from 150 to 300 K, and the DTBT temperature from 130 to 150 K (illustrated by a shaded area). Once below the transition temperature, the toughness decreases linearly to a value roughly 2% of its room temperature value. The small sized specimens were able to accurately replicate the shape of the low temperature toughness of Sn, but the test underestimates the actual impact energies.

Also displayed in Figure 2-10 are two Vitreloy 1 curves for toughness versus temperature. The first (with solid triangles) was produced in this work, while the other (open triangles) is from the literature⁴. The impact energies from literature were performed on specimens with 6x3x50 mm geometry. In both curves, the toughness decreases roughly linearly with temperature and does not exhibit a DTBT. At 100 K, Vit 1 retains 35% of its room temperature toughness, while the toughness of Sn has decreased by 98% from its room temperature toughness. The rate of Vit 1's decrease in toughness is calculated to be $\sim 0.02 \text{ J cm}^{-2} \text{ K}^{-1}$.

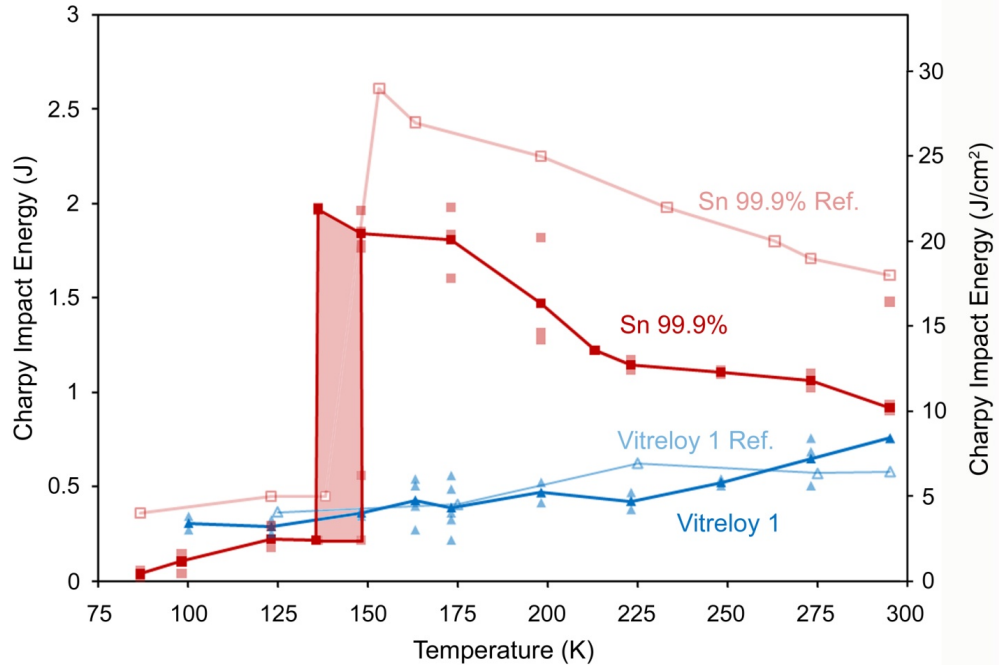


Figure 2-10: Charpy impact toughness vs. temperature for pure Sn and the BMG Vitreloy 1 compared with data obtained from References¹⁹ and⁴. The plot shows that the compact impact setup used in this work recreates the correct DBTT temperature in Sn and reproduces the shape of the curves from literature, despite the smaller specimen size. An estimate of the full-sized Charpy toughness is shown on the right axis. All the data is shown.

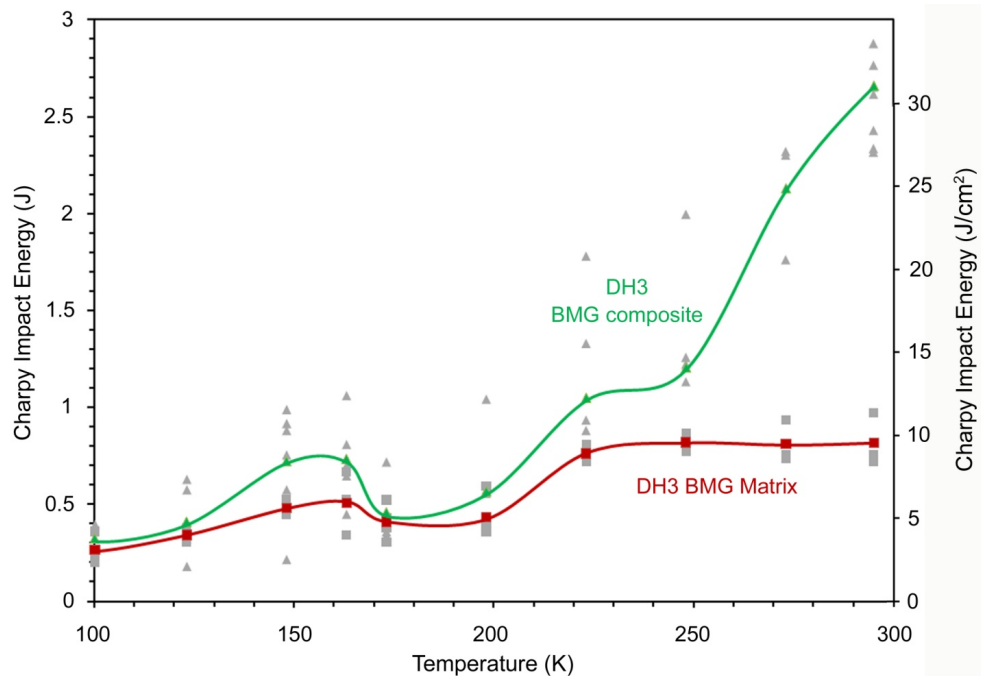


Figure 2-11: Charpy impact toughness vs. temperature for the BMGMC DH3 and its glass matrix, made separately. The curves represent the averages all of the data, which are also shown. Both alloys were produced via suction casting and notched identically.

Figure 2-11 is a plot of temperature vs. toughness for DH3, the BMGMC with 66% soft crystalline dendrite, along with an alloy which approximately mimics its glassy matrix.²⁰ The BMGMC alloy DH3 exhibits excellent room temperature toughness and ductility, but is comprised of a bcc crystalline phase that is expected to undergo a DTBT. It is known that brittle metallic phases in a glass can make the BMGMC significantly more brittle than the parent glass (as was demonstrated above). Figure 2-11 essentially confirms this hypothesis by showing that the toughness of DH3, while much higher than its matrix BMG at room temperature, quickly loses its toughness and essentially behaves like a monolithic glass. At room temperature, DH3 absorbs more than three times more energy than its glass matrix; however, the impact toughness decreases rapidly for the first 100 K of cooling due to the embrittling of the bcc dendrites. Around 175 to 200 K the DH3 and DH3-Matrix curves virtually converge, demonstrating that the matrix controls the toughness because the dendrites can no longer arrest shear band growth. DH3-Matrix exhibits a similar decrease in toughness compared to Vit 1, maintaining ~30% of its room temperature toughness at 100 K. DH3, the BMGMC, only maintains 15% of its room temperature toughness, which is obviously lower because it starts with a much higher toughness. Despite the performance, DH3's DTBT is still significantly smaller than that of Sn's, which results in only 2% toughness retention at 100 K. Both DH3 and DH3-Matrix have an impact toughness of $\sim 0.25 \text{ J}$ (2.7 J cm^{-2}), an order of magnitude higher than Sn's. Earlier in this chapter it was demonstrated that processing techniques can significantly improve the room temperature toughness of a BMGMC, however, that toughening is only worthwhile for temperatures above the DTBT. This is not necessarily a bad result; BMGMCs' superior room temperature toughness remains for the first 100 K below ambient temperature, and the amorphous matrix allows it to retain a moderate amount of toughness even at cryogenic temperatures. Therefore, the BMGMCs are never more brittle than monolithic BMGs with

decreasing temperature, and both have respectable toughness at cryogenic temperatures compared to metals that exhibit a DTBT.

Another unexpected result seen in Figure 2-11 is a slight hump in toughness around 163 K. Both DH3 and DH3-Matrix exhibit a slight increase in toughness at that temperature, followed by decreasing toughness at lower temperatures. Since the hump was observed for both alloys, it is likely a real phenomenon occurring in the glass matrix. A similar hump has not to date been observed in Vit 1, where a number of cryogenic studies have been performed.

Figure 2-12 is a collection of SEM micrographs illustrating the differences in the appearance of the fracture surface at 100, 163, and 300 K in the BMGMC DH3. Figure 2-12a-c shows micrographs from the surface of three specimens that were polished to a 0.02 μm finish prior to testing. The notch is at the top of each image, and the crack was driven downwards during impact. Figure 2-12a, a 300 K impact, exhibits a large amount of deformation and crack branching, with shear bands observed a distance of 950 μm from the edge of the crack. The typical shear band spacing, shown at two different magnifications in Figure 2-12d and e, was found to be 2.75 μm . At 163 K (Figure 2-12b) some crack branching is still apparent, although there are fewer shear bands visible on the surface (only up to 600 μm from the crack) and they have a larger spacing of 3 μm (Figure 2-12f). At 100 K (Figure 2-12c), the crack does not branch at all, and cleaves the sample without significant deformation. The few visible shear bands only extended 150 μm away from the crack, and had a spacing of 9.6 μm .

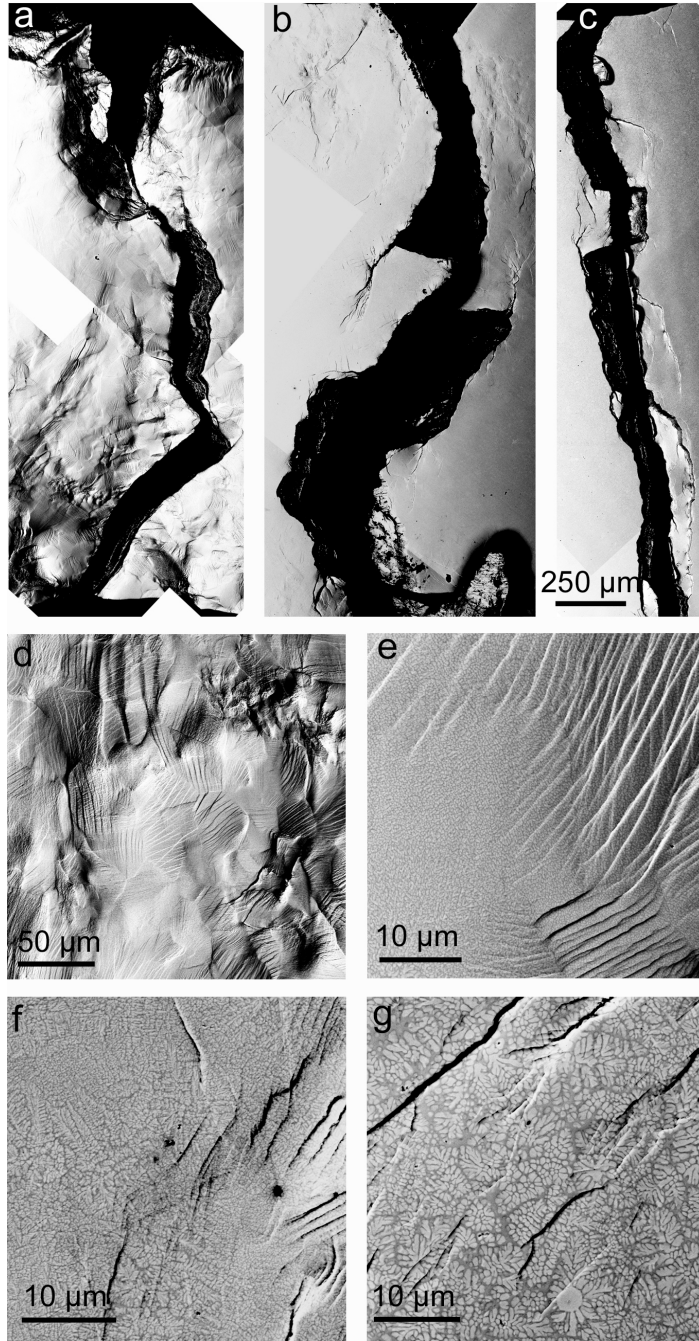


Figure 2-12: (a-c) SEM micrographs from the surface of polished Charpy specimens in the BMGMC DH3 showing how the crack morphology changes with temperature. (a) 300K, (b) 163 K, and (c) 100 K. (d-e) Enlarged micrographs of the shear bands on the surface of the DH3 sample impacted at room temperature. Similar images are shown for cryogenic specimens, (f) 163 K and (g) 100 K.

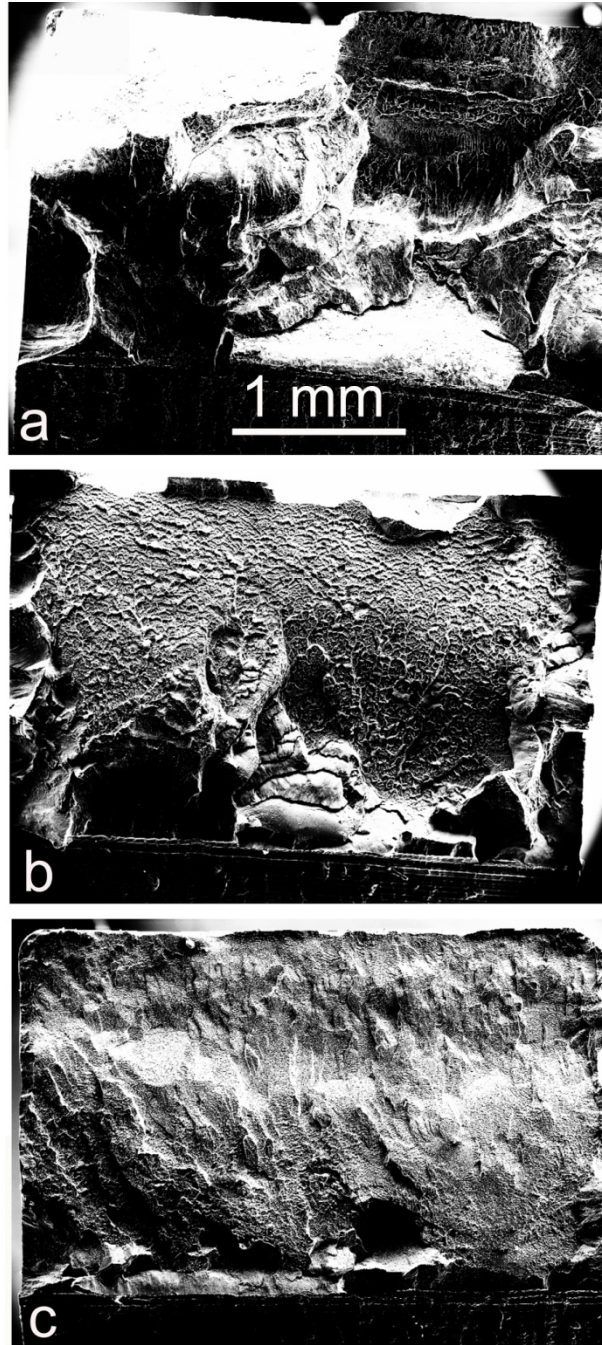


Figure 2-13: (a) SEM micrograph of the fracture surface from the monolithic BMG DH3-Matrix impacted at 300K. (b) DH3-Matrix 100 K. (c) Fracture surface from BMGMC DH3 at 100 K. In all samples the notch is at the bottom of the images.

Plastic flow of a material is a thermally activated process, so, by reducing the temperature, the number of shear bands which can be formed should decrease. Another assessment of toughness is the length of the crack-edge per mm of sample, called l , obtained from Figure 2-12a-c. In a perfectly brittle fracture, no crack branching would be observed, and the crack would travel perpendicular to the sample, leading to $l = 1$. In a tough material, the crack turns due to blunting and plastic shielding, leading to $l > 1$. In the coldest sample, impacted at 100 K, $l = 1.10$ mm/mm. At 163 K, $l = 1.38$ mm/mm, and at 300 K, $l = 1.36$ mm/mm. The lowest temperature impact has the shortest crack path, with the crack only traveling an extra 10% of distance in the material versus a pure cleavage fracture. The two higher temperature impacts both had similar crack lengths, although they had significantly different average energies of fracture. The higher concentration of shear bands in the 300 K sample can explain its higher toughness. Fracture surfaces of DH3 and DH3-Matrix are shown in Figure 2-13 at (a) 300 K and (b) 100 K. As expected, as the temperature during fracture decreases the fracture surface decreases in roughness, correlating with the decrease in toughness. Figure 2-13c is the fracture surface from DH3 at 100 K. It can be seen to be similar to the DH3-Matrix, as its surface is fairly smooth and lacks a large amount of roughness.

The final alloy tested was the Ti-based BMGMC DV1, which has a lower volume fraction of dendrites than DH3 (40%), but still is reinforced with a bcc phase. Five impacts at 100 K and 300 K were performed. The average impact energy at 100 K was found to be 0.33 J (3.7 J cm^{-2}), compared with 1.31 J (14.5 J cm^{-2}) for the 300 K sample.

Table 2-2: Summary of DH3 DTBT impacts

Temperature [K]	Shear Band Spacing [μm]	Max Shear Band Distance from Crack [μm]	l [mm/mm]	CIT [J]	CIT [J/cm^2]
100	9.6	150	1.10	0.32	3.6
163	3.0	600	1.38	0.72	8.5
300	2.75	950	1.36	2.66	29.6

CIT is Charpy impact toughness, and l is the crack-edge per mm of sample.

Conclusions

In this study a series of miniaturized Charpy experiments were performed. The influence of processing on the microstructure of BMGMCs was used to vary the microstructure of the two alloys DV1 and DH3. Their impact toughness was measured to be greatest when semisolidly forged. This technique allowed for much greater dendrite refinement than suction casting, which, in turn, increased impact toughness. The commercially cast LM2, while a BMGMC, performed poorly. This was due to the growth of a brittle crystalline phase within the amorphous matrix, with similar results to the massive decrease in toughness experienced by DH3-xtal. With proper fabrication, DV1 and DH3 can absorb more impact energy than Ti-6Al-4V, Al-2024, and Al-7075.

Impact toughness was also measured across a range of temperatures for Vitreloy 1, DH3, DH3-matrix, and Sn. The measurements for Vitreloy 1 and Sn matched well with the values from the literature. Vitreloy 1 was found to slowly decrease in toughness as the impact temperature was reduced. Sn experienced a DTBT between 130 to 150 K. DH3-matrix's temperature sensitivity was similar to Vitreloy 1's, with a gradual decrease as the temperature was reduced. DH3 was very tough at ambient temperatures. It suffered rapid degradation upon cooling, but always performed at least as well as its amorphous matrix. This study demonstrated

how even when a bcc crystal undergoes a DTBT it remains possible to mitigate the effects by constraining its failure within another tough material.

References

- (1) ASTM Standard E23, 2007, "Standard Test Methods for Notched Bar Impact Testing of Metallic Materials" **2007**.
- (2) Nayar, A. *Testing of Metals*; McGraw-Hill Education, 2005; p. 202.
- (3) Raghavan, R.; Murali, P.; Ramamurty, U. Ductile to brittle transition in the Zr₄₁Ti₁₃Cu_{12.5}Ni₁₀Be_{22.5} bulk metallic glass. *Intermetallics* **2006**, *14*, 1051–1054.
- (4) Raghavan, R.; Murali, P.; Ramamurty, U. On factors influencing the ductile-to-brittle transition in a bulk metallic glass. *Acta Mater.* **2009**, *57*, 3332–3340.
- (5) Li, H.; Tao, K.; Fan, C.; Liaw, P. K.; Choo, H. Effect of temperature on mechanical behavior of Zr-based bulk metallic glasses. *Appl. Phys. Lett.* **2006**, *89*, 041921.
- (6) Huang, Y.; Shen, J.; Sun, J.; Zhang, Z. Enhanced strength and plasticity of a Ti-based metallic glass at cryogenic temperatures. *Mater. Sci. Eng. A* **2008**, *498*, 203–207.
- (7) Yu, P.; Wang, R. J.; Zhao, D. Q.; Bai, H. Y. Anomalous temperature dependent elastic moduli of Ce-based bulk metallic glass at low temperatures. *Appl. Phys. Lett.* **2007**, *91*, 201911.
- (8) Qiao, J. W.; Liaw, P. K.; Zhang, Y. Ductile-to-brittle transition of in situ dendrite-reinforced metallic-glass–matrix composites. *Scr. Mater.* **2011**, *64*, 462–465.
- (9) Cheng, J. L.; Chen, G.; Xu, F.; Du, Y. L.; Li, Y. S.; Liu, C. T. Correlation of the microstructure and mechanical properties of Zr-based in-situ bulk metallic glass matrix composites. *Intermetallics* **2010**, *18*, 2425–2430.
- (10) Lim, K. R.; Na, J. H.; Park, J. M.; Kim, W. T.; Kim, D. H. Enhancement of plasticity in Ti-based metallic glass matrix composites by controlling characteristic and volume fraction of primary phase. *J. Mater. Res.* **2010**, *25*, 2183–2191.
- (11) Park, J. M.; Jayaraj, J.; Kim, D. H.; Mattern, N.; Wang, G.; Eckert, J. Tailoring of in situ Ti-based bulk glassy matrix composites with high mechanical performance. *Intermetallics* **2010**, *18*, 1908–1911.

- (12) Guo, S. F.; Liu, L.; Li, N.; Li, Y. Fe-based bulk metallic glass matrix composite with large plasticity. *Scr. Mater.* **2010**, *62*, 329–332.
- (13) Zhu, Z.; Zhang, H.; Hu, Z.; Zhang, W.; Inoue, a. Ta-particulate reinforced Zr-based bulk metallic glass matrix composite with tensile plasticity. *Scr. Mater.* **2010**, *62*, 278–281.
- (14) Qiao, J. W.; Feng, P.; Zhang, Y.; Zhang, Q. M.; Liaw, P. K.; Chen, G. L. Quasi-static and dynamic deformation behaviors of in situ Zr-based bulk-metallic-glass-matrix composites. *J. Mater. Res.* **2010**, *25*, 2264–2270.
- (15) Hofmann, D. C.; Suh, J.-Y.; Wiest, A.; Duan, G.; Lind, M.-L.; Demetriou, M. D.; Johnson, W. L. Designing metallic glass matrix composites with high toughness and tensile ductility. *Nature* **2008**, *451*, 1085–9.
- (16) Shin, H. S.; Kim, K.-H.; Oh, S.-Y. Fracture behavior of Zr-based bulk metallic glass under impact loading. *Int. J. Mod. Phys. B* **2006**, *20*, 4359–4364.
- (17) Shin, H.; Kim, K.; Jung, Y.; Ko, D. Impact fracture behavior of Zr-based bulk metallic glass using subsize Charpy specimen. *Adv. Fract. Strength* **2005**, *297-300*, 1356–1361.
- (18) Hofmann, D. C.; Kozachkov, H.; Khalifa, H. E.; Schramm, J. P.; Demetriou, M. D.; Vecchio, K. S.; Johnson, W. L. Semi-solid induction forging of metallic glass matrix composites. *JOM* **2009**, *61*, 11–17.
- (19) Ratchev, P.; Vandevælde, B.; Verlinden, B.; Allaert, B.; Werkhoven, D. Brittle to Ductile Fracture Transition in Bulk Pb-Free Solders. *IEEE Trans. Components Packag. Technol.* **2007**, *30*, 416–423.
- (20) Duan, G.; Wiest, A.; Lind, M. L.; Li, J.; Rhim, W.-K.; Johnson, W. L. Bulk Metallic Glass with Benchmark Thermoplastic Processability. *Adv. Mater.* **2007**, *19*, 4272–4275.